Journal of Organometallic Chemistry 752 (2014) 17–24

Contents lists available at ScienceDirect

Journal of Organometallic Chemistry

journal homepage: www.elsevier.com/locate/jorganchem

Heterobimetallic o-vanillin functionalized complexes: *In vitro* DNA binding validation, cleavage activity and molecular docking studies of Cu^{II}–Sn_2^{IV} analogs

Sartaj Tabassum [a,*], Shipra Yadav [a], Iqbal Ahmad [b]

[a] Department of Chemistry, Aligarh Muslim University, Aligarh 202002, India
[b] Department of Agricultural Microbiology, Faculty of Agricultural Sciences, Aligarh Muslim University, Aligarh 202 002, India

ARTICLE INFO

Article history:
Received 12 September 2013
Received in revised form
2 November 2013
Accepted 19 November 2013

Keywords:
Cu^{II}–Sn_2^{IV} complex
In vitro DNA profiling
5′-AMP
Oxidative cleavage
Topo I inhibition
Molecular docking

ABSTRACT

The heterobimetallic chemical entities **1**–**4** of o-vanillin functionalized Schiff base have been synthesized and characterized by elemental analysis and spectroscopic methods *viz.*, UV–vis, IR, ESI–mass, NMR (in **2** and **4**) and EPR (in **1** and **3**). The Ni^{II}–Sn_2^{IV} analogs were synthesized only for structural elucidation by NMR spectroscopy. To evaluate the biological preference with the molecular target DNA, interaction of the Cu^{II}–Sn_2^{IV} entities **1** and **3** with CT DNA has been explored by employing various biophysical methods revealing the electrostatic mode of binding *via* oxygen of sugar–phosphate backbone of DNA helix. The K_b values of **1** and **3** were found to be 2.31×10^4 and 3.67×10^4 M^{-1}, respectively suggesting the greater binding propensity of **3**. Furthermore, site of action was ascertained by the interaction studies of **1** and **3** with 5′-AMP employing UV–vis titrations, ^1H and ^{31}P NMR studies which implicates the preferential selectivity of these complexes to N1 of adenosine moiety. Moreover, the antimicrobial activities of **1** and **3**, revealed **3** as a good antimicrobial agent. The cleavage activity of **3** was evaluated by agarose gel electrophoresis assay with pBR322 DNA, revealing the involvement of singlet oxygen species *via* oxidative cleavage pathway. Additionally, **3** exhibited significant inhibitory effects on the catalytic activity of Topo I at a very low concentration, 15 μM, suggesting that **3** is an efficient catalytic inhibitor of human Topo I. The computer-aided molecular docking techniques were carried out to ascertain the mode of action toward the molecular target DNA and Topo I for **1** and **3**.

1. Introduction

Cancer is leading cause of mortality globally, accounting for 7.6 million deaths around the world in 2008, and an estimated 13.1 million deaths by 2030 [1]. The serendipitous discovery of cisplatin, cis-diamminedichloroplatinum (II) – an archetypical inorganic anticancer drug [2], has triggered the design of new improved metal-based chemotherapeutic agents with fewer side effects. The role of cisplatin, its second generation analogs *viz.*, carboplatin, oxaliplatin, etc. and multinuclear complexes like BBR3464 as chemotherapeutic anticancer drugs have been well established [3]. However, the clinical effectiveness of the existing anticancer drugs was not good enough owing to severe side effects [4] and acquisition of resistance by tumor cells [5]. To address these limitations, optimization of the chemical entities to exert effective chemotherapeutic potential was needed.

The chemotherapeutic anticancer drugs exert their cytotoxic effect, and thereby therapeutic effect by interacting with DNA, topoisomerases or DNA–topoisomerase complexes. DNA Topo I is a ubiquitous cellular enzyme that catalyzes the topological changes of DNA during fundamental cellular processes such as replication, transcription, recombination and repair by triggering single-stranded breaks in DNA [6]. Topoisomerase targeting compounds are considered as an attractive target for design of cancer chemotherapeutics, because they can cause permanent DNA damage that triggers a series of cellular events, inducing apoptosis leading to cell death [7]. In this respect, DNA Topo I inhibitors represent a class of anticancer agents forming the basis of many chemotherapy combinations widely used in a broad spectrum of tumors. A series of drugs that specifically target DNA Topo I, such as camptothecin (CPT) and its derivatives, as well as other non-CPT Topo I inhibitors like indenoisoquinolines have been used clinically as antitumor agents in cancer chemotherapy [8].

Abbreviations: CT DNA, calf thymus DNA; EB, ethidium bromide; En, ethylenediamine; Topo I, topoisomerase I; UV–vis, UV–visible.

* Corresponding author. Tel.: +91 9358255791.
E-mail addresses: tsartaj62@yahoo.com, tsartaj62@gmail.com (S. Tabassum).

0022-328X/$ – see front matter © 2013 Elsevier B.V. All rights reserved.
http://dx.doi.org/10.1016/j.jorganchem.2013.11.023

The ligand design plays a decisive role in transporting and addressing the molecule to the target, resisting untimely exchanges with biomolecules [9]. Previous literature reports have demonstrated that Schiff bases derived from o-vanillin are biologically more significant due to their superior chelating ability, structural flexibility [10] and diverse biological activities including antimicrobial [11] and antitumor [12]. Further, the potency and selectivity of o-vanillin Schiff base derivative could provide an active pharmacophore scaffold for the design of chemotherapeutic drugs [12].

Organotin(IV) complexes have displayed remarkable *in vitro* and *in vivo* antiproliferative properties, owing to which they play a crucial role in cancer oncology [13]. Further, organotin(IV) complexes with Schiff base ligands have received considerable attention owing to their fascinating chemical behavior, kinetically stable, relatively lipophilic nature and possessing attractive properties such as lower toxicity than platinum drugs [14]. While copper– an essential bioelement involved in cellular respiration, antioxidant defense, neurotransmission, connective tissue and DNA biosynthesis. Cu^{II} complexes possess diverse structures and have a high nucleobase affinity that enables them to cleave DNA effectively, which gives them potential value in the treatment of cancer [15]. On other hand, organotin(IV) compounds have demonstrated high antitumor activity *in vitro* in a wide variety of human tumors and it has been found that the organotin(IV) moiety bound preferentially to a phosphate group of the DNA backbone. Additionally, it has also been established that organotin(IV) are involved in cancer chemotherapy because of their apoptotic inducing property [16]. Further, the use of o-vanillin in association with 2-amino-2-methylpropane-1,3-diol ligand proved as good scaffold due to its potential binding modes to metal center as well as participation in hydrogen bonding interactions, which are necessary for DNA binding and Topo I inhibition.

Our interest focuses on the design of bioactive chemical entities where two or more metal centers can be incorporated in a single complex so as to achieve bifunctional architectures, preferably divalent copper with organotin(IV), which produces a highly cationic species that exerts strong electrostatic attraction to the anionic phosphate backbone of DNA. Such metalated chemical entities (with two or more active metal centers) act synergistically to cleave DNA with higher efficiency and also exhibit preferential intrinsic DNA interactions inside the cell that make them interesting for continued investigation of their reactivity with DNA.

2. Experimental

2.1. Materials and measurements

Reagent grade chemicals were used without further purification for all syntheses and experiments. Ethylenediamine (Loba Chem.), 2-hydroxy-3-methoxybenzaldehyde (o-vanillin), 2-amino-2-methylpropane-1,3-diol, dimethyltin(IV) dichloride, diphenyltin(IV) dichloride, tris buffer {Tris(hydroxymethyl)aminomethane}, NaN_3, DMSO, SOD, methyl green, DAPI (Sigma–Aldrich), copper(II) chloride dihydrate, nickel(II) chloride hexahydrate (E. Merck), 6X loading dye (Fermentas Life Science), 5′-AMP (Fluka), doxycycline, nystatin (Hi-Media) supercoiled plasmid pBR322 DNA (Genei) and Topo I (CalBioChem) were utilized as received. Disodium salt of CT (calf thymus) DNA purchased from Sigma Chem. Co. and was stored at 4 °C.

The ^{1}H, ^{13}C and ^{119}Sn NMR spectra were obtained on a Bruker DRX-400 spectrometer operating at 400, 100 and 150 MHz, respectively. Infrared spectra were recorded on Interspec 2020 FTIR spectrometer in KBr pellets from 400 to 4000 cm^{-1}. Electrospray mass spectra were recorded on Micromass Quattro II triple quadrupol mass spectrometer. Microanalyses (C, H and N) were performed on an Elementar Vario EL III. EPR spectra of copper complexes were recorded on Varian E 112 spectrometer at the X-band frequency (9.1 GHz). Electronic spectra were recorded on a UV-1700 PharmaSpec UV–vis Spectrophotometer (Shimadzu). Fluorescence measurements were made on Shimadzu RF–5301PC Spectrofluorophotometer. Viscosity measurements were carried out from observed flow time of CT DNA containing solution ($t > 100$ s) corrected for the flow time of buffer alone (t_0), using Ostwald's viscometer at 25 ± 0.01 °C. Flow time was measured with a digital stopwatch. Molar conductance was measured at room temperature on Eutech con 510 electronic conductivity bridge.

2.2. DNA binding and cleavage experiments

DNA binding experiments which include absorption spectral titrations, fluorescence titrations and viscosity measurements conformed to the standard methods and practices previously adopted by our laboratory [17–20]. DNA cleavage experiment has been performed by the standard protocol [21].

2.3. Topoisomerase I inhibition assay

One unit of the enzyme was defined as completely relax 1 μg of negatively supercoiled pBR322 DNA in 30 min at 310 K under the standard assay conditions. The reaction mixture (30 μL) contained 35 mM Tris–HCl (pH 8.0), 72 mM KCl, 5 mM $MgCl_2$, 5 mM DTT, 2 mM spermidine, 0.1 mg/ml BSA, 0.25 μg pBR322 DNA, 2 Unit Topo I and complex **3**. These reaction mixtures were incubated at 310 K for 30 min, and the reaction was terminated by addition of 4 μL of 5× buffer solution consisting of 0.25% bromophenol blue, 4.5% SDS and 45% glycerol. The samples were electrophoresed through 1% agarose in TBE at 30 V for 8 h.

2.4. Molecular docking studies

The rigid molecular docking studies were performed by using HEX 6.3 software [22], which is an interactive molecular graphics program for calculating and displaying feasible docking modes of pairs of protein, enzymes and DNA molecule. The structure of the complex was sketched by CHEMSKETCH (http://www.acdlabs.com) and converted to pdb format from mol format by OPENBABEL (http://www.vcclab.org/lab/babel/). The crystal structure of the B-DNA dodecamer $d(CGCGAATTCGCG)_2$ (PDB ID: 1BNA) and human–DNA Topo I complex (PDB ID: 1SC7) was downloaded from the protein data bank (http://www.rcsb.org./pdb). Visualization of the docked pose has been done by using CHIMERA (www.cgl.ucsf.edu/chimera) molecular graphics program.

2.5. Antimicrobial assays

2.5.1. Antibacterial activity

The heterobimetallic Cu^{II}–Sn_2^{IV} analogs **1** and **3** were screened for *in vitro* antibacterial activity against two Gram-negative [*Escherichia coli* (ATCC 25922) and *Pseudomonas aeruginosa* (ATCC 27853)] and two Gram-positive [*Staphylococcus aureus* (ATCC 25923) and *Bacillus subtilis* (MTCC 121)] bacterial strains. The agar well diffusion method was adopted for determining zones of inhibition [23]. Briefly, all cultures were routinely maintained on NA (nutrient agar) and incubated at 37 °C overnight. The culture was centrifuged at 1000 rpm and pellets were resuspended and diluted in sterile normal saline solution to obtain viable count 10^5 cfu/ml. Volume of 0.1 ml of diluted bacterial culture suspension was spread uniformly with the help of spreader on NA plates. Wells of 8 mm size were cut and loaded with different concentrations of the test complexes. Antibiotic disc, doxycycline (30 μg/disc) and solvent

were used as positive and negative control respectively. The plates were then incubated for 24 h at 37 °C, and the resulting zones of inhibition (in mm) were measured.

2.5.2. Antifungal activity

All cultures were routinely maintained on SDA and incubated at 28 °C. The inoculums of non-sporing fungi, *Candida albicans* were performed by growing the culture in SD broth at 37 °C for overnight. Volume of 0.1 ml of diluted fungal culture suspension was spread with the help of spreader on SDA plates uniformly. Sterile 8 mm discs were impregnated with the test compounds. Wells of 8 mm size were cut and loaded with different concentrations of the test samples. Antibiotic disc, nystatin (30 μg/disc) were used as positive control. *C. albicans* plates were incubated at 37 °C for 18–48 h. Antifungal activity was determined by measuring the diameters of the inhibition zone.

2.6. Syntheses

*2.6.1. Synthesis of ligand, **L***

The Schiff base ligand, **L** was synthesized from 2-amino-2-methylpropane-1,3-diol (1.051 g, 10 mmol) and o-vanillin (1.52 g, 10 mmol) by adopting the reported procedure [12].

2.6.2. Synthesis of $[Cu(en)_2]Cl_2$ and $[Ni(en)_2]Cl_2$

The monometallic complexes of $[Cu(en)_2]Cl_2$ and $[Ni(en)_2]Cl_2$ were synthesized by adding ethylenediamine (1.34 ml, 20 mmol) in a methanolic solution of $CuCl_2\cdot 2H_2O$ (1.70 g, 10 mmol)/$NiCl_2\cdot 6H_2O$ (2.38 g, 10 mmol) in a 2:1 molar ratio as described in the earlier reported procedure [24].

*2.6.3. Synthesis of heterobimetallic complexes **1**–**4***

Methanolic solution of dimethyltin dichloride (0.87 g, 4 mmol)/diphenyltin dichloride (1.37 g, 4 mmol) was added to a stirring methanolic solution of $[Cu(en)_2]\cdot Cl_2$ (0.50 g, 2 mmol)/$[Ni(en)_2]\cdot Cl_2$ (0.49 g, 2 mmol). The reaction mixture was kept on reflux on water bath for ca. 2 h, the reaction was monitored by TLC. To this methanolic solution of ligand, **L** (0.956 g, 4 mmol) was added drop wise and the resulting solution was continued to reflux for 6 h. Depending upon the Cu^{II}/Ni^{II} complex, blue or green colored solids, respectively were precipitated out which were filtered, washed with diethyl ether and dried *in vacuo*.

Complex 1: Yield, 68%. M.p. 260 °C (decompose). Anal. Calc. for $C_{32}H_{56}N_6O_8CuSn_2$ (%) C, 40.29; H, 5.91; N, 8.81. Found: C, 40.07; H, 5.69; N, 8.37. Selected IR data (cm^{-1}/υ): 3332 υ(OH); 3186 υ(N–H), 1573 δ(N–H); 1629 υ(C=N); 1231 υ(C–O); 566 υ(Sn–C); 538 υ(Sn–O); 470 υ(Cu–N); 433 υ(Sn–N). Molar Conductance, Λ_M (10^{-3} M, DMSO): 21 Ω^{-1} cm^2 mol^{-1} (non electrolyte). UV–vis (DMSO, λ_{max}, nm): 553, 382, 274. ESI–MS (*m*/*z*, DMSO): 865.1 $[C_{32}H_{56}N_6O_8CuSn_2 - 2C_4H_9O_2 + H]^+$.

Complex 2: Yield, 63%. M.p. >300 °C (decompose). Anal. Calc. for $C_{32}H_{56}N_6O_8NiSn_2$ (%) C, 40.50; H, 5.94; N, 8.85. Found: C, 40.43; H, 5.81; N, 8.49. Selected IR data (cm^{-1}/υ): 3334 υ(OH); 3192 υ(N–H), 1577 δ(N–H); 2922 $\upsilon_s(CH_2)$, 2847 $\upsilon_{as}(CH_2)$; 1630 υ(C=N); 1236 υ(C–O); 576 υ(Sn–C); 530 υ(Sn–O); 467 υ(Ni–N); 432 υ(Sn–N). Molar Conductance, Λ_M (10^{-3} M, DMSO): 24 Ω^{-1} cm^2 mol^{-1} (non electrolyte). UV–vis [DMSO, λ_{max}, nm]: 546, 428, 383, 272. ^{1}H NMR (400 MHz, DMSO-d_6, δ ppm): 9.87 (2H, azomethine CH=N), 7.6–7.3 (6H, Ar–H), 3.58 (6H, O–CH_3), 2.13 (8H, ethylenediamine –CH_2), 1.18 (6H, **L** –CH_3), 0.91 (6H, Sn–CH_3). ^{13}C NMR (100 MHz, DMSO-d_6, δ ppm): 163.25 (2C, C=N), 132.07–114.27 (12C, Ar–C), 63.58 (4C, **L** CH_2–OH), 57.84 (2C, **L** –OCH_3), 39.92 (4C, ethylenediamine –CH_2), 17.62 (2C, **L** –CH_3), 9.21 (4C, Sn–CH_3). ^{119}Sn-NMR (150 MHz, DMSO-d_6, δ ppm): –243. ESI–MS (*m*/*z*, DMSO): 862.9 $[C_{32}H_{56}N_6O_8NiSn_2 - 2C_4H_9O_2 + H]^+$.

Complex 3: Yield, 61%. M.p. 290 °C (decompose). Anal. Calc. for $C_{52}H_{64}N_6O_8CuSn_2$ (%) C, 51.96; H, 5.36; N, 6.99. Found: C, 51.37; H, 5.31; N, 6.50. Selected IR data (cm^{-1}/υ): 3326 υ(OH); 3181 υ(N–H), 1579 δ(N–H); 2919 $\upsilon_s(CH_2)$, 2841 $\upsilon_{as}(CH_2)$; 1628 υ(C=N); 1233 υ(C–O); 556 υ(Sn–C); 533 υ(Sn–O); 470 υ(Cu–N); 444 υ(Sn–N). Molar Conductance, Λ_M (10^{-3} M, DMSO): 27 Ω^{-1} cm^2 mol^{-1} (non electrolyte). UV–vis [DMSO, λ_{max}, nm]: 557, 385, 273. ESI–MS (*m*/*z*, DMSO): 1111.1 $[C_{52}H_{64}N_6O_8CuSn_2 - 2C_4H_9O_2 + 2H]^+$.

Complex 4: Yield, 58%. M.p. >300 °C (decompose). Anal. Calc. for $C_{52}H_{64}N_6O_8NiSn_2$ (%) C, 52.17; H, 5.38; N, 7.01. Found: C, 52.01; H, 5.18; N, 6.91. Selected IR data (cm^{-1}/υ): 3329 υ(OH); 3178 υ(N–H), 1583 δ(N–H); 2926 $\upsilon_s(CH_2)$, 2843 $\upsilon_{as}(CH_2)$, 1631 υ(C=N); 1228 υ(C–O); 560 υ(Sn–C); 539 υ(Sn–O); 468 υ(Ni–N); 446 υ(Sn–N). Molar Conductance, Λ_M (10^{-3} M, DMSO): 32 Ω^{-1} cm^2 mol^{-1} (non electrolyte). UV–vis [DMSO, λ_{max}, nm]: 542, 431, 380, 275. ^{1}H NMR (400 MHz, DMSO-d_6, δ ppm): 9.88 (2H, azomethine CH=N), 7.7–7.01 (Ar–H), 3.61 (6H, O–CH_3), 2.13 (8H, ethylenediamine –CH_2), 1.18 (6H, **L** –CH_3). ^{13}C NMR (100 MHz, DMSO-d_6, δ ppm): 161.21 (2C, C=N), 117.54–146.51 (24C, **L** + SnPh Ar–C), 64.23 (4C, **L** CH_2–OH), 48.67 (2C, **L** –OCH_3), 39.72 (4C, ethylenediamine –CH_2), 17.68 (2C, **L** –CH_3). ^{119}Sn-NMR (150 MHz, DMSO-d_6, δ ppm): –256. ESI–MS (*m*/*z*, DMSO): 1107.2 $[C_{52}H_{64}N_6O_8NiSn_2 - 2C_4H_9O_2 + H]^+$.

3. Results and discussion

3.1. Synthesis and characterization

The synthetic route of new organotin(IV) analogs, **1**–**4** is represented in Scheme 1. The proposed structures were formulated on the basis of their elemental analysis, spectroscopic techniques (IR, NMR, ESI–MS, UV–vis and EPR) and molar conductance values. The molar conductivity data of synthesized complexes **1**–**4** in DMSO (10^{-3} M) at 25 °C were too low to account for any dissociative ions in the complexes, consistent with their non-electrolytic nature.

The IR spectrum of non-coordinated Schiff base ligand, **L** exhibits medium absorption band at 1637 cm^{-1} attributable to azomethine υ(C=N), which was perturbed to lower frequencies by 9–6 cm^{-1} upon complexation in **1**–**4** indicating donation of the lone pair of azomethine nitrogen to Sn atom. The characteristic stretching vibration of the phenolic oxygen ν(C–O) was shifted to lower frequencies in the 1236–1228 cm^{-1} in **1**–**4**, suggesting involvement of phenolic oxygen in coordination after deprotonation [25]. A medium intensity band at 3400–3300 cm^{-1} attributable to the –NH_2 group of ethylenediamine disappeared completely in all complexes **1**–**4** and new bands appeared at 3192–3178 and 1583–1570 cm^{-1} corresponding to ν(N–H) stretching and δ(N–H) bending vibrations, respectively, supporting the coordination of ethylenediamine to Cu^{II}/Ni^{II} and subsequently to Sn^{IV} metal ions by the elimination of HCl [26]. Furthermore, the diagnostic assignments of **1**–**4** corresponding to υ(Sn–C), υ(Sn–O) and υ(Sn–N) were found at 576–556, 539–530 and 446–432 cm^{-1}, respectively [27]. Besides, all the complexes exhibited a sharp band in the region 478–467 cm^{-1} attributed to υ(Cu/Ni–N) vibrations supporting the coordination through nitrogen.

In the NMR spectra, the assignment of the proton resonances was made by their peak multiplicity, intensity pattern and comparison of the integration values of the protons with the expected composition. The ^{1}H NMR spectra of **2** and **4** recorded in DMSO-d_6 demonstrated the absence of –OH signal at δ ~12.6 ppm indicating the involvement of phenolic –OH group in coordination to Sn^{IV} metal center through deprotonation [28]. The characteristic signal of –HC=N group at δ 9.87 and 9.88 ppm in **2** and **4**, respectively, revealed a significant chemical shift due to ligation of nitrogen atom to tin metal centers. In case of dimethyltin analog **2**, the

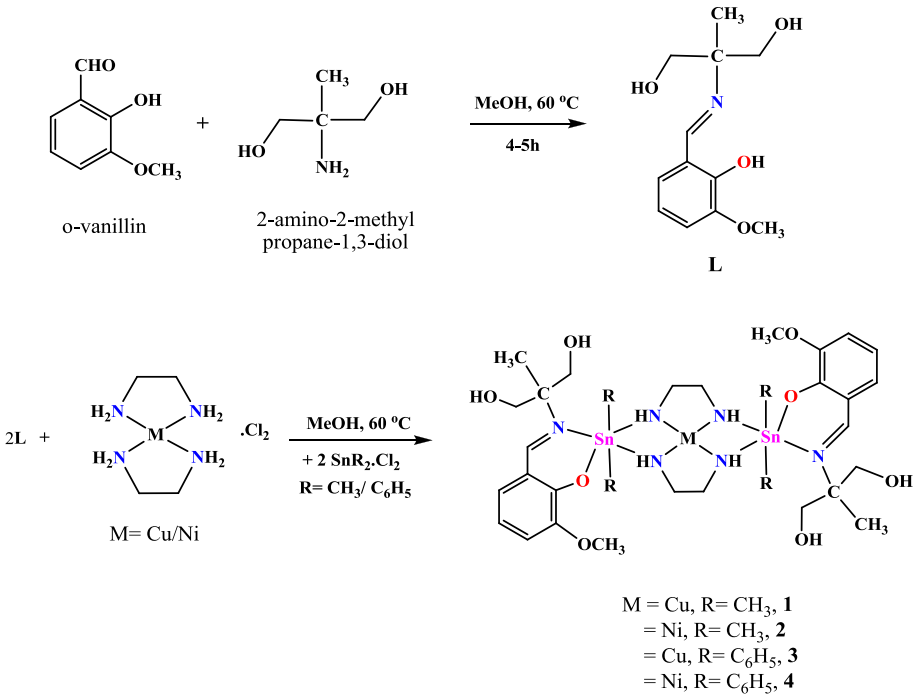

Scheme 1. Schematic representation of synthetic route for the complexes **1**–**4**.

presence of methyl group bound to tin atom was confirmed as a singlet at δ 0.91 ppm. Other resonance signals at δ 2.13 and 2.42 ppm in **2** and **4**, respectively, corresponds to $-CH_2$ protons of ethylenediamine moiety.

The ^{13}C NMR spectra of **2** and **4** revealed signals at δ 63.58 and 64.23 ppm, respectively attributable to $-\underline{C}H_2-OH$ of 2-amino-2-methylpropane-1,3-diol moiety, at $\delta \sim 39$ and 146.51–114.27 ppm corresponding to the ethylenediamine $-CH_2$ and aromatic carbons, respectively.

The ^{119}Sn NMR spectra of complexes exhibited a sharp singlet indicating the formation of a single species. The spectra of **2** and **4** exhibited ^{119}Sn NMR resonances at -243 and -256 ppm, respectively, supported hexacoordinate geometry around Sn^{IV} metal ions [29].

The EPR spectra of Cu^{II}–Sn_2^{IV} analogs **1** and **3** were recorded in DMSO at LNT. The X-band EPR spectra of **1** exhibited anisotropic signal with $g_{||} = 2.17$, $g_{\perp} = 2.08$ and $g_{av} = 2.11$ computed from the expression $g_{av}^2 = (g_{||}^2 + 2g_{\perp}^2)/3$. Similarly, **3** exhibited these values at $g_{||} = 2.15$, $g_{\perp} = 2.06$ and $g_{av} = 2.09$. These parameters are consistent with the values reported for other related square planar Cu^{II} systems and are typical of axially symmetrical d^9 Cu^{II} complexes [30]. In square planar complexes, the unpaired electron lies in the d_z^2 orbital giving $^2A_{1g}$ as the ground state with $g_{\perp} > g_{||} > 2.0023$, while giving $^2B_{1g}$ with $g_{||} > g_{\perp} > 2.0023$, if the unpaired electron lies in the d_{x-y}^{22} orbital. From the observed values, it was clear from the trend $g_{||} > g_{\perp} > 2.0023$, that the unpaired electron was predominantly in the d_{x-y}^{22} orbital of the Cu^{II} ion.

The electronic absorption spectra can often provide quick and reliable information about the ligand arrangement in transition metal complexes. The electronic spectra of the chemical entities **1**–**4** were recorded in DMSO at room temperature in the range of 190–1100 nm exhibited characteristic absorption bands in the range of 272–275 nm which could be attributed to intraligand $\pi \rightarrow \pi^*$ transitions. Other low energy $n \rightarrow \pi^*$ transition bands of non-bonding electrons of azomethine nitrogen of the Schiff base ligand were observed at 380–385 nm. The Cu^{II}–Sn_2^{IV} entities **1** and **3** were characterized by a broad band at 553 and 557 nm, respectively assignable to $^2B_{1g} \rightarrow {}^2A_{1g}$ transitions, which strongly favor square planar geometry around the Cu^{II} ion [31]. While, the diamagnetic Ni^{II}–Sn_2^{IV} entities exhibited d → d transitions at 546 and 428 nm in case of complex **2** and 542 and 431 nm in case of complex **4**, corresponding to $^1A_{1g} \rightarrow {}^1B_{1g}$ and $^1A_{1g} \rightarrow {}^1A_{2g}$ transitions, respectively consistent with the square planar geometry around the Ni^{II} center [32].

Since refractive single crystals of the complexes could not be obtained, the crystalline nature of the chemical entities **1**–**4** was authenticated by XRPD measurements. The diffractograms obtained for the metal complexes **1**–**4** are given.

3.2. DNA binding studies

3.2.1. Electronic absorption spectroscopy

The UV–vis spectra of heterobimetallic Cu^{II}–Sn_2^{IV} entities **1** and **3** exhibited increase in the absorption intensities (hyperchromism, 23 and 37%, respectively) of ligand–centered $\pi \rightarrow \pi^*$ absorption band at $\sim$274 nm without any appreciable shift in band positions (Fig. 1). The intrinsic binding constants (K_b) of the complexes were determined by monitoring the changes in the absorbance at the intraligand band with increasing concentrations of CT DNA. The observed "hyperchromic" effect revealed the electrostatic mode of interaction of complexes with DNA. Since both the complexes **1** and **3** possess a heterobimetallic core Cu^{II}–Sn_2^{IV} which offers dual mode of binding *viz.*; coordinate covalent binding of Cu^{II} ion to N7 of guanine [33] and Sn^{IV} ions shows preference for the oxygen atoms of vicinal phosphate moiety of DNA double helix [34], therefore, synergic bonding interaction can be envisaged for these complexes. The K_b values of **1** and **3** were found to be 2.31×10^4 and 3.67×10^4 M^{-1}, respectively. The results revealed that the diphenyltin analog **3** exhibits stronger DNA binding propensity as compared to dimethyltin analog **1**, which could be attributed to the more intimate binding of phenyl moiety into the DNA helix. Moreover, free –OH groups of the complexes, encourage the groove binding by engaging in hydrogen-bonding with the functional groups positioned on the edge of DNA bases which feature novelty

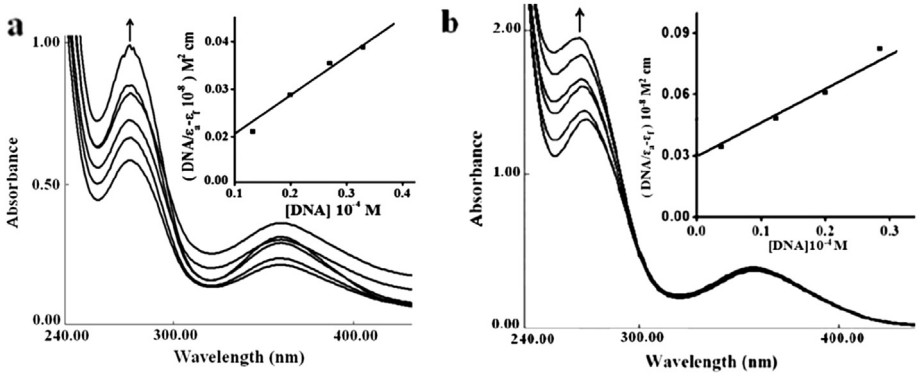

Fig. 1. Absorption spectra of complexes (a) **1** and (b) **3** in the presence of increasing amount of CT DNA. Inset: Plots of [DNA]/($\varepsilon_a - \varepsilon_f$) vs. [DNA] for the titration of CT DNA with complexes. [Complex] = 1.3×10^{-4} M, [CT DNA] = 0–1.2×10^{-4} M.

as it provides molecular recognition at the specific target site at the cellular level [35].

3.2.2. Interaction with 5′-AMP

The UV–vis absorption titrations of **1** and **3** with 5′-AMP in DMSO were carried out to investigate the specific recognition of complexes with the nucleobases/phosphate sugar backbone of DNA helix. As shown, addition of increasing amounts of 5′-AMP to complexes **1** and **3**, resulted in hyperchromism with a blue shift of ~2 nm which was suggestive of the binding of **1** and **3** to 5′-AMP through electrostatic interactions. The K_b values were calculated for **1** and **3** and were found to be 1.74×10^4 and 2.87×10^4 M^{-1}respectively, consistent with UV–vis results. Further to validate our hypothesis of **1** and **3** showing preferential binding toward the AT– rich sequence of DNA, interaction studies of **1** and **3** with 5′-AMP were carried out by ^{1}H and ^{31}P NMR techniques at physiological pH 7.2. The ^{1}H NMR of free 5′-AMP in D_2O exhibits H2 and H8 aromatic protons (adjacent to N7 and N1 atom of adenine, respectively) resonance at 7.83 and 8.12 ppm, respectively. On addition of **1** to 5′-AMP, the H2 signal shifted to 8.02 ppm, while H8 signal undergoes a significant shift at 8.36 ppm, while upon addition of **3** the H2 and H8 signals shifted to 8.18 and 8.50 ppm, respectively, suggesting the stronger binding affinity of **3** to 5′-AMP as compared to **1**. These significant shifts result due to the deshielding of H8 proton by coordinate bond formation of Cu^{II} ions of **1** and **3** preferably *via* N1 atom rather than N7 of 5′-AMP [36].

The ^{31}P NMR signal appeared in free 5′-AMP at 0.72 ppm, and exhibited slight shift (0.83 and 0.87 ppm with 5′-AMP) in presence of **1** and **3**, respectively indicating the involvement of Sn^{IV} ion binding with the phosphate backbone of DNA.

3.2.3. Fluorescence studies

Fluorescence spectral technique is an effective method to study metal interaction with DNA. Since, the complexes **1** and **3** exhibited strong fluorescence at ~385 nm in 0.01 Tris–HCl/50 mM NaCl buffer when excited at 270 nm at physiological pH, fixed amounts of **1** and **3** were titrated with increasing amounts of CT DNA. The addition of CT DNA exhibited gradual enhancement in fluorescence emission intensity without any change in the position of the emission bands, which implied that chemical entities revealed strong interactions with DNA as illustrated in Fig. 2. The enhancement of the emission intensity is mainly due to the change in the environment of metal complex and is related to the extent to which complex is inserted into the hydrophobic environment inside the DNA helix; which reduces the accessibility of solvent molecules at the binding site and thus preventing the quenching effect [37]. Thus, it is evident that complexes were protected efficiently by the DNA helix, leading to decrease in the vibrational modes of relaxation and higher emission intensity. The binding constant, *K* estimated for **1** and **3** by Scatchard equation were found to be 2.03×10^4 and 3.10×10^4 M^{-1}, respectively and followed similar trend as in the case of absorption spectral studies.

3.2.4. Ethidium bromide displacement assay

In order to further investigate the interaction mode and binding affinities of the complexes **1** and **3** with DNA, quenching

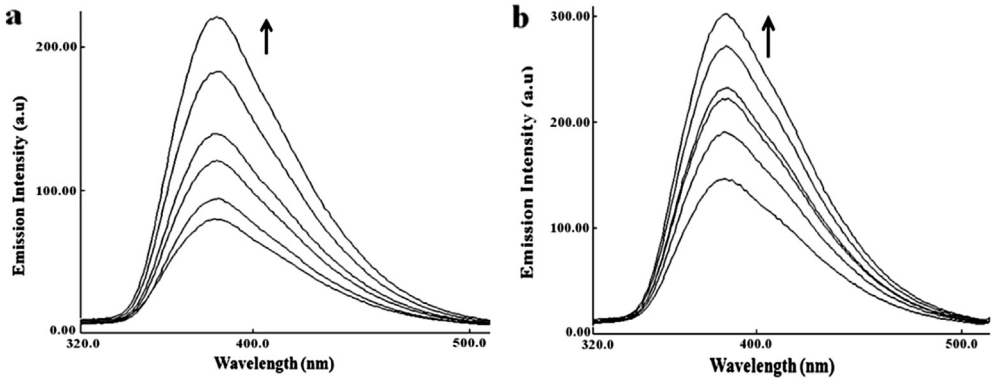

Fig. 2. Emission spectra of complexes (a) **1** and (b) **3** in Tris–HCl buffer (pH = 7.2) in the absence and presence of CT DNA. [Complex] = 1.3×10^{-4} M, [DNA] = 0–0.50×10^{-4} M. Arrows indicate the change in emission intensity upon increasing the DNA concentration.

experiments with EB were employed. The EB displacement technique is based on the decrease of fluorescence resulting from the displacement of EB from a DNA sequence by a quencher, and the quenching is due to the reduction of the number of binding sites on the DNA that is available to the EB. The increasing concentrations of the complexes **1** and **3** (0–1.2×10^{-4} M) to DNA pretreated with EB ([DNA]/[EB] = 1) (0.2×10^{-4} M) resulted in remarkable quenching of the emission intensity, indicative of the competitive displacement of the bound EB from the CT–DNA by the complexes. The relative binding propensity of the complexes to DNA is measured from the extent of reduction in the emission intensity. As complexes **1** and **3** bind to DNA through electrostatic binding mode *via* the phosphate backbone of DNA helix, the observed quenching may be due to the photoelectron transfer mechanism [38]. The K_{sv} values calculated from Stern–Volmer equation for complexes **1** and **3** were found to be 0.64 and 1.06, respectively. The greater decrease in the K_{sv} value for complex **3** compared to complex **1** was attributed to the strong binding of the complex with DNA double helix.

3.2.5. Effect of ionic strength

To evaluate the electrostatic contribution into the DNA-binding event of the complexes **1** and **3**, the effect of the ionic strength on the emission spectrum of complexes was monitored. The fluorescence intensity of DNA bound complexes was moderately quenched with increasing ionic strength through added NaCl (0–0.50×10^{-4} M). Due to the competitive interaction for phosphate anions, the addition of NaCl weakens the surface binding interactions as well as hydrogen bonding between the CT DNA and the interacting molecules [39].

3.2.6. Viscosity measurements

The plots of relative viscosities vs. [complex]/[DNA] are shown. The relative specific viscosity of the DNA reduces steadily upon addition of Cu^{II}–Sn^{IV}_2 analogs **1** and **3** support our contention that the complexes bind to DNA *via* non-covalent interactions [40]. The decreased relative viscosity of DNA may be explained by a binding mode which produced bends or kinks in the DNA strand, thereby diminishing its effective length and concomitantly its viscosity.

3.3. DNA cleavage studies of pBR322 DNA

Since, **3** exhibited greater binding propensity to CT DNA, the cleavage activity of **3** was studied using supercoiled plasmid pBR322 DNA as a substrate in a medium of 5 mM Tris–HCl/50 mM NaCl buffer (pH 7.2) under physiological conditions. A concentration dependent DNA cleavage by **3** was performed at increasing complex concentrations (10–50 μM) which exhibiting significant cleavage at 50 μM without the formation of Form III, suggesting single strand DNA cleavage.

The mechanistic aspects of the DNA cleavage reaction of **3** were studied in the presence of radical scavengers. The DNA cleavage in the presence of hydroxyl radical scavengers (DMSO and EtOH), singlet oxygen quencher (NaN_3) and SOD as superoxide radical scavenger is shown in Fig. 3a. An enhancement in the DNA cleavage was observed upon the addition of DMSO and EtOH, ruling out the involvement of hydroxyl radical in the cleavage process (Fig. 3a, Lanes 2 and 3). Since, no obvious inhibition was observed in the presence of SOD, the possibility of involvement of superoxide radical in DNA cleavage was ruled out (Fig. 3a, Lane 4). While, in the presence of NaN_3, DNA cleavage is significantly inhibited which was indicative of the involvement of the singlet oxygen or a singlet oxygen-like entity in the cleavage process (Fig. 3a, Lane 5). This inhibitory activity of NaN_3 can be ascribed to the affinity of the azide anion for transition metals [41].

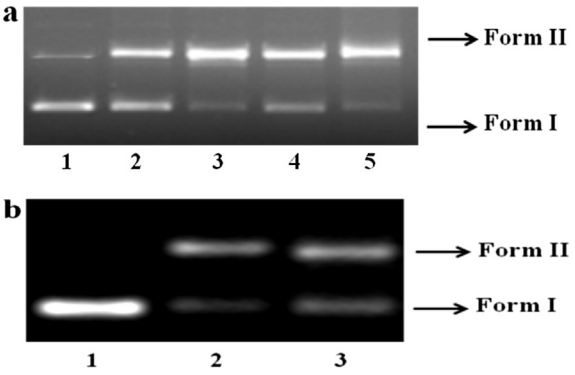

Fig. 3. Agarose gel electrophoresis pattern for the cleavage of pBR322 supercoiled DNA (300 ng) by complex **3** in presence of (**a**) different activating agents at 310 K after incubation for 45 min. Lane 1: DNA Control; Lane 2: 50 μM of complex + DMSO (0.4 M) + DNA; Lane 3: 50 μM of complex + EtOH (0.4 M) + DNA; Lane 4: 50 μM of complex + SOD (15 units) + DNA Lane 5: 50 μM of complex + sodium azide (0.4 M) + DNA (**b**) DNA recognition agents at 310 K after incubation for 45 min. Lane 1, DNA control; Lane 2, 40 μM of complex **1** + DNA + methyl green (2.5 μL of a 0.01 mg/ml solution); Lane 3, 40 μM of complex **1** + DNA + DAPI (8 μM).

From the results obtained above we may suggest that **3** is capable of promoting DNA cleavage through an oxidative DNA damage pathway. A copper peroxide with DNA cleaving ability is formed by an active singlet oxygen species or a singlet oxygen-like entity. The assumed involvement of copper–oxo species can be deduced from the reaction of copper(I) and endogenous dioxygen to give superoxide anion that dismutates, giving rise to hydrogen peroxide that can react yielding copper(I) to obtain a copper–oxo species [42].

The DNA groove binding preference of **3** was studied using DNA major groove binder methyl green and DNA minor groove binder distamycin. A significant inhibition in the chemical nuclease activity of **3** was observed in the presence of distamycin, while methyl green addition exhibited no apparent effect on the DNA cleavage (Fig. 3b). These results are of significance as majority of the oxidative cleavage reagents generally bind in the minor groove rather than major groove [43].

3.4. Topoisomerase I inhibition

Topo I inhibitors inhibit or reduce the rate of religation in the DNA cleavage complex and ultimately leads to cell death after collision of the cleavage complex, with the replication fork resulting in double-strand breakage [44]. The gel electrophoresis pattern was obtained by incubating pBR322 DNA with Topo I in the presence of different concentrations of **3**. As shown in Fig. 4, supercoiled DNA was fully relaxed by the enzyme in the absence of **3** (Lane 2). However, upon increasing the concentrations of **3** (7.5–15 μM), the levels of the relaxed form (OC) were inhibited (Lanes 3–6) [45]. At 15 μM the DNA relaxation effect caused by Topo I was completely inhibited by **3**. These observations suggest that **3** inhibits Topo I catalytic activity due to the relatively strong DNA binding affinity of the complex, preventing the enzyme from efficiently binding to DNA.

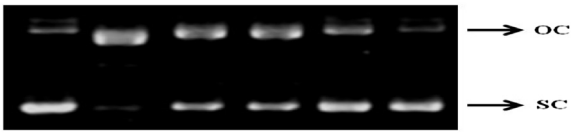

Fig. 4. Agarose gel electrophoresis pattern showing effect of different concentration of complex **3** on the activity of DNA Topo I; Lane 1, DNA control; Lane 2, Topo I + DNA; Lane 3, 7.5 μM of complex + DNA + Topo I; Lane 4: 10 μM of complex + DNA + Topo I; Lane 5: 12.5 μM of complex + DNA + Topo I; Lane 6: 15 μM of complex + DNA + Topo I.

4. Molecular docking

4.1. Molecular docking with DNA

Computer-aided molecular docking studies of **1** and **3** with DNA duplex of sequence d(CGCGAATTCGCG)$_2$ dodecamer (PDB ID: 1BNA) were carried out in order to predict the chosen binding site along with preferred orientation of the chemical species inside the DNA minor groove (Fig. 5a and b). The results exhibited that **1** and **3** interact with DNA *via* an electrostatic mode involving outside edge stacking interactions with the oxygen atom of the phosphate backbone of DNA. Moreover, –OH groups of the complexes acts as strong H–bond donor or acceptor and were found to be engaged in hydrogen-bonding interactions with DNA nucleobases available in the minor grooves. The minimum energy docked pose revealed that **1** and **3** preferentially bind to the minor groove of double-stranded DNA, within A–T regions of the dodecamer, thus making favorable hydrogen bonding and electrostatic interactions with DNA functional groups that define the stability of groove [46]. Further, **1** and **3** supported the structural complementarity of the DNA minor groove of AT–DNA, as its floor is smooth and convex, while the floor of GC-sequences is interrupted by the exocyclic amino groups of guanines protruding into the groove and obstructing good fit of a minor groove-binder. The resulting relative binding energy of docked complexes **1** and **3** with DNA were found to be −252.2 and −272.8 kJ mol^{-1} respectively.

Thus, we can conclude that there is a mutual complement between spectroscopic studies and molecular docking techniques, which can substantiate our experimental results and at the same time provides further evidence of groove binding.

4.2. Molecular docking with human–DNA Topo I

To further validate the exact binding site of Topo I inhibition, **1** and **3** were successively docked with the human–DNA Topo I complex (PDB ID: 1SC7). The X-ray crystallographic structure of the human–DNA Topo I complex (PDB ID: 1SC7) was uploaded in which Topo I is bound to the oligonucleotide sequence 5′–AAAAAGACTTsX-GAAAATTTTT-3′, where 's' is 5′-bridging phosphorothiolate of the cleaved strand and 'X' represents any of the four bases A, G, C or T. The phosphoester bond of G12 in 1SC7 was rebuilt and SH of G11 on the scissile strand was changed to OH [47]. The resulting docking model (Fig. 6a) indicated that the complex **1** failed to search the exact binding site of Topo I–DNA complex,

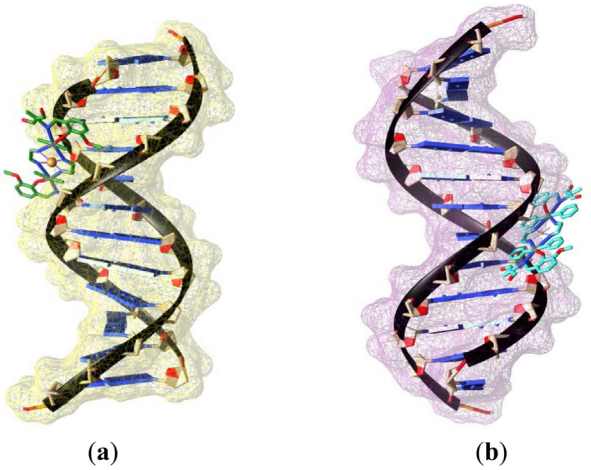

Fig. 5. Molecular docked model of complex (a) **1** and (b) **3** with DNA dodecamer duplex of sequence d(CGCGAATTCGCG)$_2$ (PDB ID: 1BNA).

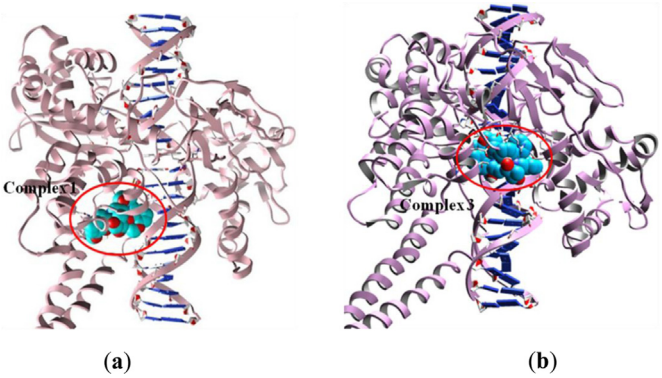

Fig. 6. (a) Molecular docked model of complex **1** was failed to target the cleavage active site of human DNA Topo I (PDB ID: 1SC7) and (b) Complex **3** targeting in the cleavage active site of human DNA Topo I (PDB ID: 1SC7).

thereby unable to block the rewinding step of the phosphoester bond of G12, while **3** approached toward the DNA cleavage site in the Topo I–DNA complex forming a stable complex (Fig. 6b). The insertion of **3** into the Topo I–DNA cleavage complex increases the distance between ends of the broken DNA strand and prevents relegation resulting in prolonged attachment of Topo I to DNA. The –OH groups of the ligand in **3** was involved in H-bond with the scissile strand, which could strongly block the religation process, subsequently leads to inhibitory effect on Topo I [48]. The resulting docked model with minimum relative binding energy of −330 kJ mol^{-1} demonstrates **3** as an efficient Topo I inhibitor. Thus, molecular docking studies provide a structural explanation of binding mode of the metal complex in the active site of an enzyme.

5. Antimicrobial activity

In vitro screening tests of synthesized Cu^{II}–Sn^{IV}_2 chemical entities **1** and **3** were carried out for their antibacterial and antifungal activity. The results shown in Fig. 7 indicated that **3** (diphenyltin derivative) exhibited a higher activity against all tested bacteria as compared to **1** (dimethyltin derivative). This higher antibacterial

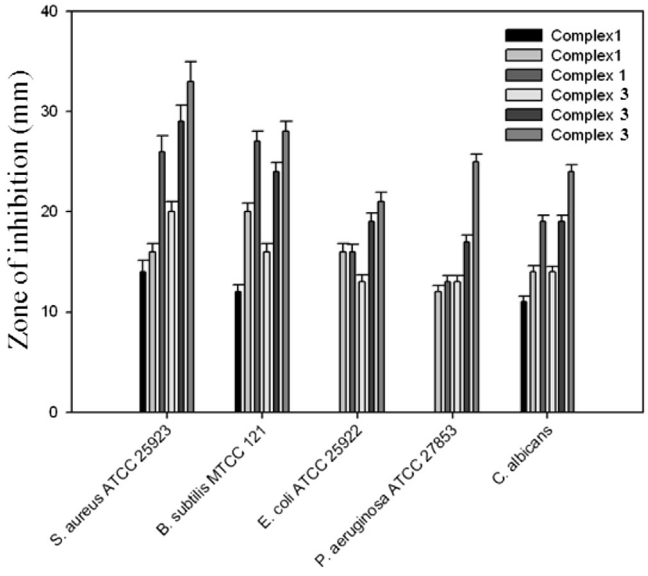

Fig. 7. Antimicrobial activity of complexes **1** and **3** against different bacterial strains, at varying concentrations (250, 500 and 1000 μg/ml). The maximum inhibition zone is represented by the reference drug.

activity of **3** against most of bacteria strains could be attributed to the high lipophilic character of diphenyltin moiety. The presence of two phenyl groups in **3** increases the solubility of the complex in lipids and hence it can cross through biological membranes with higher efficiency [49]. However, both **1** and **3**, exhibited lesser activity than the reference drug (doxycyclin).

The synthesized compounds were also screened for their antifungal activity against *C. albicans*. The results demonstrated that both the Cu^{II}–Sn_2^{IV} DNA binding agents **1** and **3** exhibited good antifungal activity.

6. Conclusions

This work describes the synthesis and characterization of heterobimetallic Cu^{II}/Ni^{II}–Sn_2^{IV} chemical entities **1**–**4**, derived from o-vanillin Schiff base. The comparative *in vitro* DNA binding profile of **1** and **3** was investigated by absorption, fluorescence and viscosity measurements and the results revealed electrostatic interactions along with the selective binding to the minor groove of DNA. The intrinsic binding constant, K_b revealed higher binding propensity of diphenyltin analog, **3** as compared to dimethyltin analog, **1**. The antimicrobial activity of **1** and **3** was evaluated which revealed that **3** exhibited better antimicrobial activity than **1**. Further, the pBR322 DNA cleaving ability of **3** was evaluated by agarose gel electrophoresis which revealed that the complex bind to double-stranded DNA possibly in the minor groove and cleaves supercoiled DNA through an oxidative cleavage mechanism induced by a reactive oxygen species. Furthermore, **3** exhibited significant inhibitory effects on Topo I activity. Additionally, molecular docking studies of **1** and **3** were performed with molecular target DNA and the active site of topoisomerase enzyme in order to validate the experimental results. Therefore, from the above results it could be concluded the introduction of diphenyltin moiety could significantly enhance the activity both in DNA binding and Topo I inhibition, thereby complex **3** proving its worth as a robust and better choice for potent and safe chemotherapeutic drug design.

Acknowledgments

The authors are grateful to *SAIF*, Panjab University, Chandigarh; *STIC*, Cochin and IIT Bombay, India for providing ESI–MS, NMR, elemental analysis and EPR facility, respectively. They also acknowledge financial support to the Department of Chemistry, AMU through UGC assisted DRS–SAP and DST PURSE Programme.

References

[1] Cancer; Fact Sheet No. 297, World Health Organization, Geneva, Switzerland; http://www.who.int/mediacentre/factsheets/fs297/en/index.html.
[2] B. Rosenberg, L. Van camp, Cancer Res. 30 (1970) 1799–1802.
[3] K.S. Lovejoy, S.J. Lippard, Dalton Trans. (2009) 10651–10659.
[4] L.R. Kelland, Drugs 59 (2000) 1–8.
[5] V. Srb, E. Kubzova, K. Kubikova, Neoplasma 33 (1986) 615–620.
[6] J.J. Champoux, Annu. Rev. Biochem. 70 (2001) 369–413.
[7] Y. Pommier, Chem. Rev. 109 (2009) 2894–2902.
[8] Y. Pommier, E. Leo, H.L. Zhang, C. Marchand, Chem. Biol. 17 (2010) 421–433.
[9] A. Alama, B. Tasso, F. Novelli, F. Sparatore, Drug Discov. Today 14 (2009) 500–508.
[10] Y. Zou, W.-L. Liu, C.-S. Lu, L.-L. Wen, Q.-J. Meng, Inorg. Chem. Commun. 7 (2004) 985–987.
[11] M.S. Nair, R.S. Joseyphus, Spectrochim. Acta Part A 70 (2008) 749–753.
[12] S. Tabassum, S. Amir, F. Arjmand, C. Pettinari, F. Marchetti, N. Masciocchi, G. Lupidi, R. Pettinari, Eur. J. Med. Chem. 60 (2013) 216–232.
[13] M. Gielen, E.R.T. Tiekink, Metallotherapeutic Drugs and Metal Based Diagnostic Agents. The Use of Metals in Medicine, J. Wiley & Sons, 2005, pp. 421–439.
[14] T.S. Basu Baul, S. Basu, D. de Vos, A. Linden, Invest. New Drugs 27 (2009) 419–431.
[15] R. Buchtik, Z. Travnicek, J. Vanco, R. Herchel, Z. Dvorak, Dalton Trans. 40 (2011) 9404–9412.
[16] S. Tabassum, S. Mathur, F. Arjmand, K. Mishra, K. Banerjee, Metallomics 4 (2012) 205–217.
[17] J. Marmur, J. Mol. Biol. 3 (1961) 208–218.
[18] M.E. Reicmann, S.A. Rice, C.A. Thomas, P. Doty, J. Am. Chem. Soc. 76 (1954) 3047–3053.
[19] A. Wolfe, G.H. Shimer, T. Meehan, Biochemistry 26 (1987) 6392–6396.
[20] J.R. Lakowiez, G. Webber, Biochemistry 12 (1973) 4161–4170.
[21] F. Arjmand, S. Parveen, D.K. Mohapatra, Inorg. Chim. Acta 388 (2012) 1–10.
[22] D.W. Ritche, V. Venkataraman, Bioinformatics 26 (2010) 2398–2405.
[23] A. Rehman, M.I. Choudhary, W.J. Thomsen, Bioassay Techniques for Drug Development, Harwood Academic Publishers, Amsterdam, The Netherlands, 2001, p. 9.
[24] G. Wilkinson, R.D. Gillard, J.A. McCleverty, Comprehensive Coordination Chemistry, Peragamon Press, Oxford, 1987, pp. 516–550.
[25] K. Nakamoto, Infrared and Raman Spectra of Inorganic and Coordination Compounds, third ed., John Wiley & Sons, New York, 1986.
[26] G.F. deSousa, V.M. Deflon, M.T.P. Gambardella, R.H.P. Francisco, J.D. Ardisson, E. Niquet, Inorg. Chem. 45 (2006) 4518–4525.
[27] F. Arjmand, I. Yousuf, J. Organomet. Chem. 743 (2013) 55–62.
[28] I. Kaya, A. Bilici, M. Gul, Polym. Adv. Technol. 19 (2008) 1154–1163.
[29] R. Zhang, J. Sun, C. Ma, J. Organomet. Chem. 690 (2005) 4366–4372.
[30] S. Srinivasan, P. Athappan, G. Rajagopal, Trans. Met. Chem. 26 (2001) 588–593.
[31] H. Unver, Z. Hayvali, Spectrochim. Acta Part A 75 (2010) 782–788.
[32] F. Arjmand, B. Mohani, S. Ahmad, Eur. J. Med. Chem. 40 (2005) 1103–1110.
[33] S. Tabassum, S. Yadav, F. Arjmand, J. Organomet. Chem. 745–746 (2013) 226–234.
[34] M. Chauhan, F. Arjmand, J. Organomet. Chem. 692 (2007) 5156–5164.
[35] M. Baldini, M.-B. Ferrari, F. Bisceglie, G. Pelosi, S. Pinelli, P. Tarasconi, Inorg. Chem. 42 (2003) 2049–2055.
[36] R. Jastrzab, J. Inorg. Biochem. 103 (2009) 766–773.
[37] S. Kashanian, M.B. Gholivand, F. Ahmadi, A. Taravati, A.H. Colagar, Spectrochim. Acta Part A 67 (2007) 472–478.
[38] B. Selvakumar, V. Rajendiran, P.V. Maheswari, H.S. Evans, M. Palanaindavar, J. Inorg. Biochem. 100 (2006) 316–330.
[39] F.-Y. Wu, F.-Y. Xie, Y.-M. Wu, J.-I. Hong, J. Fluoresc. 18 (2008) 175–181.
[40] U. Chaveerach, A. Meenongwa, Y. Trongpanich, C. Soikum, P. Chaveerach, Polyhedron 29 (2010) 731–738.
[41] F.B. ElAmrani, L. Perelló, J.A. Real, M.G. Alvarez, G. Alzuet, J. Borrás, S.G. Granda, J.M. Bernardo, J. Inorg. Biochem. 100 (2006) 1208–1218.
[42] D.-D. Li, J.-L. Tian, W. Gu, X. Liu, H.-H. Zeng, S.-P. Yan, J. Inorg. Biochem. 105 (2011) 894–901.
[43] W.K. Pogozelski, T.D. Tullius, Chem. Rev. 98 (1998) 1089–1107.
[44] Y. Pommier, P. Pourquier, Y. Urasaki, J. Wu, G.S. Laco, Drug Resist. Updat. 2 (1999) 307–318.
[45] B. Montaner, W.C. Avila, M. Martinell, R. Ollinger, J. Aymami, E. Giralt, R.P. Tomas, Toxicol. Sci. 85 (2005) 870–879.
[46] J.-T. Wang, Q. Xia, X.-H. Zheng, H.-Y. Chen, H. Chao, Z.-W. Mao, L.-N. Ji, Dalton Trans. 39 (2010) 2128–2136.
[47] X.S. Xiao, S. Antony, Y. Pommier, M. Cushman, J. Med. Chem. 48 (2005) 3231–3238.
[48] H.T.M. Van, W.-J. Cho, Bioorg. Med. Chem. Lett. 19 (2009) 2551–2554.
[49] T.S.B. Baul, Appl. Organomet. Chem. 22 (2008) 195–204.